
SubTrack++ : Gradient Subspace Tracking for Scalable LLM Training

Sahar Rajabi Nayeema Nonta Sirisha Rambhatla
University of Waterloo, Waterloo, Canada
{srajabi, nonta, sirisha.rambhatla}@uwaterloo.ca

Abstract

Training large language models (LLMs) is highly resource-intensive due to their massive number of parameters and the overhead of optimizer states. While recent work has aimed to reduce memory consumption, such efforts often entail trade-offs among memory efficiency, training time, and model performance. Yet, true democratization of LLMs requires simultaneous progress across all three dimensions. To this end, we propose SubTrack++ that leverages Grassmannian gradient subspace tracking combined with projection-aware optimizers, enabling Adam’s internal statistics to adapt to changes in the optimization subspace. Additionally, employing recovery scaling, a technique that restores information lost through low-rank projections, further enhances model performance. Our method demonstrates SOTA convergence by exploiting Grassmannian geometry and achieves lowest evaluation loss, **outperforming the current SOTA while reducing pre-training wall time by 43%** and maintaining the memory footprint on a 1B-parameter Llama model.

1 Introduction

Large Language Models (LLMs) have demonstrated state-of-the-art performance across a wide range of tasks and are rapidly growing in popularity. However, training and fine-tuning these models require significant resources, including extensive hardware and time, which limits their practicality for many applications and increases their environmental impact and carbon footprint. [Zhao et al., 2024, Jaiswal et al., 2024, Muhamed et al., 2024, Miles et al., 2024, Modoranu et al., 2024, Hao et al., 2024, Li et al., 2024].

Several techniques have been proposed to mitigate memory bottlenecks, such as gradient checkpointing [Chen et al., 2016] and memory offloading [Rajbhandari et al., 2020]. LoRA [Hu et al., 2021] and other low-rank adaptation methods [Dettmers et al., 2024, Hu et al., 2021, Yaras et al., 2024, Lialin et al., 2023, Renduchintala et al., 2024, Xia et al., 2024, Miles et al., 2024] have gained popularity by optimizing a reduced set of parameters. Such approaches often assume that the full parameter space is inherently low-rank—an assumption that does not always hold and can lead to suboptimal performance. In addition, methods like BAdam [Luo et al., 2024] and Block-LLM [Ramesh et al., 2024], utilize block coordinate descent to optimize parameter subsets, achieving memory savings at the cost of partial parameter tuning and reduced accuracy.

However, memory requirements extend beyond trainable parameters, with a significant portion consumed by optimizers for storing element-wise states [Zhao et al., 2024]. To address this, recent efforts have focused on reducing the optimizer parameters while still targeting full parameter training [Li et al., 2023, Anil et al., 2019, Lv et al., 2024, Dettmers et al., 2022, Zhang et al., 2024, Modoranu et al., 2024, Zhao et al., 2024, Muhamed et al., 2024, Rajabi and Rambhatla, 2024a]. Leveraging the fact that gradients evolve in a low-dimensional space during gradient descent [Gur-Ari et al., 2018, Schneider et al., 2024, Yaras et al., 2023], GaLore [Zhao et al., 2024] reduces memory usage by projecting gradients into a low-rank subspace and periodically updating the rank- r approximation

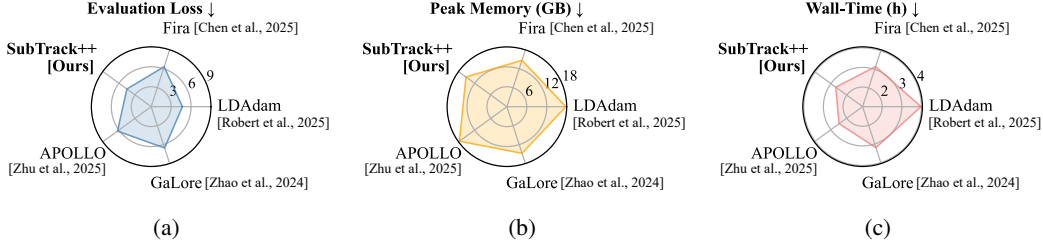


Figure 1: We compare baselines on pre-training a 1B-parameter model. (a) SubTrack++ achieves the lowest evaluation loss across all methods. (b) Its peak memory usage is significantly lower than APOLLO and LDAdam, and on par with GaLore and Fira. (c) In terms of wall-time, SubTrack++ incurs minimal overhead relative to APOLLO and is markedly faster than GaLore, Fira, and LDAdam. Overall, SubTrack++ outperforms all baselines in evaluation loss while matching or exceeding them in memory and runtime efficiency.

via singular value decomposition (SVD)—an approach also used in more recent method, Fira [Chen et al., 2025]. While SVD offers optimal low-rank approximation [Robert et al., 2025], performing it repeatedly can pose several challenges. First, it is computationally intensive, and alternatives like random projections (as in APOLLO [Zhu et al., 2025] and GoLore [He et al., 2025]) or approximation methods for estimating dominant singular values (as in LDAdam [Robert et al., 2025], Online Subspace Descent [Liang et al., 2024] and Rajabi and Rambhatla [2024b]) match or outperform SVD in practice. Moreover, SVD is sensitive to noise [Vaswani et al., 2018, He et al., 2025] and tends to degrade in late training stages when gradients are small, often hindering convergence [He et al., 2025].

Geometry-based methods have demonstrated strong performance in various machine learning applications [Zhang et al., 2018, Balzano et al., 2011, He et al., 2011, Rajabi and Rambhatla, 2024c, Blocker et al., 2023]. In this context, using Grassmannian manifolds for subspace tracking has led to structurally embedded information, lower computational complexity, and improved performance [Zhang et al., 2018, Balzano et al., 2011, He et al., 2011, Blocker et al., 2023, Chakraborty et al., 2017, Zhang and Balzano, 2016]. Grassmannian is the set of r -dimensional subspaces in a d -dimensional space, and the ultimate goal of low-rank optimization is to find the proper subspace in this space. This line of work has demonstrated robustness and efficiency in high-dimensional, noisy environments [Zhang et al., 2018, Balzano et al., 2011, He et al., 2011, Balzano et al., 2018, Chakraborty et al., 2017], outperforming online or robust Principle Component Analysis (PCA) techniques [Li, 2004, Balzano et al., 2018, Chakraborty et al., 2017]. Their natural robustness against perturbations and strong theoretical guarantees make them particularly well-suited to tracking the evolving gradient subspaces encountered in LLM training. [Balzano, 2012, Balzano et al., 2011].

To this end, we employ subspace tracking on Grassmannian geodesics (Figure 2), to develop a geometry-based, time- and memory-efficient method for tracking the gradient subspace. This way, instead of reconstructing low-rank approximations via expensive SVD or random projections, we can efficiently leverage previously computed subspaces and the estimation error to better adjust the projection. We also incorporate subspace shifts into Adam’s first and second momentum update rules, ensuring proper alignment with coordinate changes using a Projection-Aware Optimizer [Robert et al., 2025]. Additionally, we recover and scale (Recovery Scaling) the gradient information lost during low-rank projection to boost performance by utilizing the scaling information of the low-rank optimizer Chen et al. [2025], Zhu et al. [2025].

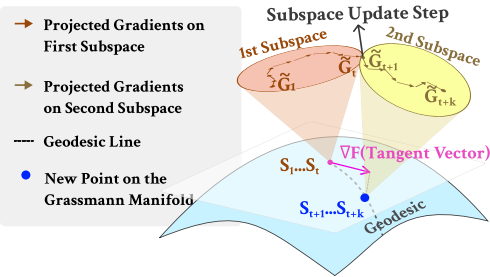


Figure 2: Visualization of Grassmannian-based subspace tracking: Between subspace updates, gradients are projected onto a fixed subspace. The tangent vector ∇F is computed via the derivative of a loss function that measures the subspace estimation error. The subspace is then updated by moving along the corresponding geodesic, determined by ∇F , on the Grassmannian manifold to minimize estimation error.

To summarize, SubTrack++ is a projection-aware geometry-based approach that supports full-parameter training and incorporates recovery scaling, offering superior time efficiency compared to SVD or PowerSGD methods (e.g., GaLore [Zhao et al., 2024], FiRA [Chen et al., 2025], LDAdam

[Robert et al., 2025]), while maintaining GaLore’s memory footprint. It outperforms online PCA methods like Online Subspace Descent [Liang et al., 2024] in subspace tracking and achieves SOTA convergence and evaluation loss across all strong baselines; Comparison provided in Figure 1.

2 SubTrack++

Challenges of Low-Rank Optimization. Projecting gradients into a low-rank subspace reduces memory overhead and enables scalable LLM training, but it introduces important trade-offs. First, gradient subspaces can be unstable and require adaptive tracking; while SVD-based methods can capture these shifts [Zhao et al., 2024, Chen et al., 2025], they are computationally expensive. To address this, recent work has explored cheaper approximations and random projections [Robert et al., 2025, Liang et al., 2024, Zhu et al., 2025, He et al., 2025]. Furthermore, optimizers like Adam assume a fixed coordinate system, so any changes in the subspace must be reflected in their internal states to preserve consistent momentum updates. Finally, low-rank projections inherently discard some gradient components, that recovering and utilizing these discarded signals can lead to improved performance [Chen et al., 2025, Zhu et al., 2025].

Overview. We propose SubTrack++ , a memory- and time-efficient method for full, simultaneous parameter tuning that embeds geometric insights into low-rank optimization. It improves efficiency and performance via three core components: 1) Subspace Tracking—Grassmannian-based updates that refine projections using estimation error and subspace history; 2) Projection-Aware Optimizer—adjusting Adam’s internal states to account for shifting subspaces; and 3) Recovery Scaling—rescaling discarded gradient components to reclaim lost information.

Subspace Tracking. In SubTrack++ , subspace estimation is framed as selecting a point on the Grassmannian—the manifold of all d -dimensional subspaces in an n -dimensional space [Bendokat et al., 2024]—which is the formal definition and goal of low-rank projections. This geometric perspective offers three key benefits: 1) By moving along Grassmann geodesics, it refines the subspace using prior subspace and estimation error, avoiding full reinitialization as done in [Zhao et al., 2024, Chen et al., 2025, He et al., 2025]. 2) Updates rely on lightweight algebraic operations, minimizing time and memory costs. 3) Controlled subspace shifts improve robustness against noise and abrupt changes.

The initial subspace is computed using SVD as shown in (1). $G_0 \in \mathbb{R}^{m \times n}$ is the gradient matrix at step 0; U , S , and V are its SVD components, and r is the specified rank.

$$G_0 = USV^\top \approx \sum_{i=1}^r s_i u_i v_i^\top \quad (1)$$

At each step, gradients are projected onto the subspace of left singular vectors if $m \leq n$, and right singular vectors otherwise; optimizing memory usage [Zhao et al., 2024]. We assume $m \leq n$ without loss of generality, so the subspace is represented by $S_t \in \mathbb{R}^{m \times r}$ ($S_0 = [u_1, \dots, u_r]$), an orthonormal basis spanning the top- r directions. The gradient is projected as $\tilde{G}_t = S_t^\top G_t \in \mathbb{R}^{r \times n}$, and the optimizer operates in this reduced space, significantly lowering memory and state overhead.

To track subspace drift, we adjust the core subspace every k steps, defined as the *subspace update interval*, by minimizing its Euclidean distance to the current gradient. The objective is formalized in the cost function (2).

$$F(S_t) = \min_A \|S_t A - G_t\|_F^2, \quad (2)$$

where A is the solution to the least squares problem. The derivative of (2) with respect to S_t is given in (3), and the residual $R = G_t - S_t A$ lies in the orthogonal complement of S_t . To update the subspace, we calculate the tangent vector ∇F on the Grassmannian, as shown in (4) based on Edelman et al. [1998], where the second equality holds because R is orthogonal to $S_t S_t^\top$.

$$\frac{\partial F}{\partial S_t} = 2(S_t A - G_t)A^\top = -2RA^\top \quad (3)$$

$$\nabla F = (I - S_t S_t^\top) \frac{\partial F}{\partial S_t} = \frac{\partial F}{\partial S_t} = -2RA^\top \approx \hat{U}_F \hat{\Sigma}_F \hat{V}_F^\top \quad (4)$$

The tangent vector ∇F provides the direction for adjusting the subspace by accounting for the error lying in the orthogonal complement. However, to minimize changes to the subspace, SubTrack++ first computes a rank-1 approximation of ∇F , determined by its largest singular value and the

Algorithm 1 SubTrack++(Subspace Tracking , Projection-Aware Optimizer , Recovery Scaling , Regular Adam)

Require: $W_t, G_t \in \mathbb{R}^{m \times n}$ with $m \leq n$ (w.l.o.g.), learning rate α , decay rates β_1 and β_2 , SubTrack++ step-size η , rank r , subspace update interval k , recovery scaling limiter factor ζ . We use \oslash to denote Hadamard division.

```
 $S_0 \leftarrow U[:, :r]$ , where  $U, S, V \leftarrow \text{SVD}(G_0)$  {Initializing First Subspace}
for  $t = 0, \dots, T$  do
  if  $t \bmod k == 0$  then
     $G_{lr} = \arg \min_A \|(S_{t-1}A - G_t)\|^2$ , and  $R = G_t - S_{t-1}G_{lr}$ 
     $\nabla F = -2RG_{lr}^\top \approx \widehat{U}_F \widehat{\Sigma}_F \widehat{V}_F^\top$ 
     $S_t = (S_{t-1} \widehat{V}_F \quad \widehat{U}_F) \begin{pmatrix} \cos \widehat{\Sigma}_F \eta \\ \sin \widehat{\Sigma}_F \eta \end{pmatrix} \widehat{V}_F^\top + S_{t-1}(I - \widehat{V}_F \widehat{V}_F^\top)$ 
     $M_t \leftarrow \beta_1 \cdot (S_t^\top S_{t-1} M_{t-1}) + (1 - \beta_1) \cdot \widetilde{G}_t$  { $\widetilde{G}_t = S_t^\top G_t$ : low-rank projection of  $G_t$ }
     $\mathcal{V}_t \leftarrow \beta_2 \cdot [(1 - \beta_2^{t-1})|(S_t^\top S_{t-1})^2 \cdot (\mathcal{V}_{t-1} - M_{t-1}^2) + (S_t^\top S_{t-1} \cdot M_{t-1})^2|] + (1 - \beta_2) \cdot \widetilde{G}_t^2$ 
  else
     $S_t = S_{t-1}$ 
     $M_t \leftarrow \beta_1 \cdot M_{t-1} + (1 - \beta_1) \cdot \widetilde{G}_t$ 
     $\mathcal{V}_t \leftarrow \beta_2 \cdot \mathcal{V}_{t-1} + (1 - \beta_2) \cdot \widetilde{G}_t^2$ 
  end if
   $\widetilde{G}_t^O = M_t \oslash \sqrt{\mathcal{V}_t + \epsilon}$ ,  $\widehat{G}_t = S_t \widetilde{G}_t^O$  { $\widetilde{G}_t^O$ : optimizer's output,  $\widehat{G}_t$ : projected-back gradients }
   $\phi_t(G_t)_i = \frac{\|\widetilde{G}_{t,i,i}^O\|}{\|\widetilde{G}_{t,i,i}\|}$ ,  $\Lambda_t = \phi_t(G_t)(G_t - S_t \widetilde{G}_t)$  {We use  $\oslash$  to denote Hadamard division.}
  if  $\frac{\Lambda_t}{\Lambda_{t-1}} > \zeta$  then  $\Lambda_t \leftarrow \frac{\Lambda_t}{\|\Lambda_t\|} \cdot \zeta \|\Lambda_{t-1}\|$ 
   $W_t \leftarrow W_{t-1} - \alpha \cdot \widehat{G}_t$   $-\alpha \cdot \Lambda_t$ 
end for
```

corresponding singular vector obtained from its SVD, and represented as $\widehat{U}_F \widehat{\Sigma}_F \widehat{V}_F^\top$ in the final equality of (4). This approximation is then used to update the subspace.

As shown by Edelman et al. [1998], Bendokat et al. [2024], from which we have included the necessary definitions and theorem in section 3, we can move along a Grassmannian geodesic guided by the computed tangent vector, taking a step of size η , as presented in (5).

$$S_{t+1}(\eta) = (S_t \widehat{V}_F \quad \widehat{U}_F) \begin{pmatrix} \cos \widehat{\Sigma}_F \eta \\ \sin \widehat{\Sigma}_F \eta \end{pmatrix} \widehat{V}_F^\top + S_t(I - \widehat{V}_F \widehat{V}_F^\top) \quad (5)$$

This update rule preserves the orthonormality of S_{t+1} , ensuring it remains on the Grassmannian. The last term in (4), projects the previous subspace onto the orthogonal complement of \widehat{V}_F , ensuring that the portion of S_t which has not been updated in this step is still included.

Projection-Aware Optimizer. In Adam, the first and second momentum update rule is shown in (6) and (7), respectively (reminder: \widetilde{G}_t is the projection of gradient into low-rank subspace).

$$M_t \leftarrow \beta_1 \cdot M_{t-1} + (1 - \beta_1) \cdot \widetilde{G}_t \quad (6)$$

$$\mathcal{V}_t \leftarrow \beta_2 \cdot \mathcal{V}_{t-1} + (1 - \beta_2) \cdot \widetilde{G}_t^2 \quad (7)$$

Inspired by methods such as LDAdam [Robert et al., 2025], we emphasize the importance of updating optimizer states in a projection-aware manner to account for shifting subspaces; otherwise, misaligned projections can distort the optimizer's performance. To address this, at each subspace update step, we modify Adam's original update rules in (6) and (7), replacing them with projection-aware counterparts represented in (8) and (9), which reflect subspace changes into optimizer statistics [Robert et al., 2025]. Further details regarding this projections can be found in Appendix C.

$$M_t \leftarrow \beta_1 \cdot (S_t^\top S_{t-1} M_{t-1}) + (1 - \beta_1) \cdot \widetilde{G}_t \quad (8)$$

$$\mathcal{V}_t \leftarrow \beta_2 \cdot [(1 - \beta_2^{t-1})|(S_t^\top S_{t-1})^2 \cdot (\mathcal{V}_{t-1} - M_{t-1}^2) + (S_t^\top S_{t-1} \cdot M_{t-1})^2|] + (1 - \beta_2) \cdot \tilde{G}_t^2 \quad (9)$$

These projection-aware update rules enables Adam optimizer to track optimization dynamics precisely as the subspace evolves, achieving significantly better practical performance.

Recovery Scaling. Optimizer outputs $\tilde{G}_t^O = M_t \oslash \sqrt{\mathcal{V}_t + \epsilon}$ (\oslash denotes Hadamard division), which is then projected back via $\hat{G}_t = S_t \tilde{G}_t^O$ to be used in weight update; however, low-rank projections inevitably discard some information in the full gradient matrix, that could enhance performance if properly utilized. Fira [Chen et al., 2025] observed that adaptive optimizers like Adam exhibit consistent scaling behaviour in low-rank and full-rank regimes. This suggests that the scaling information of the low-rank optimizer can be used to recover and rescale the discarded components of the gradient. A similar method is also employed in APOLLO [Zhu et al., 2025]. Consequently, an additional correction term is added to the standard weight update rule, as formalized in (10).

$$W_t \leftarrow W_{t-1} - \alpha \cdot \hat{G}_t - \alpha \cdot \phi_t(G_t)(G_t - S_t \hat{G}_t) \quad (10)$$

Here α is the learning rate and $\phi_t(G_t)$ is the scaling factor computed based on the low-rank gradient representation, \tilde{G}_t , and the optimizer’s processed output, \tilde{G}_t^O as:

$$\phi_t(G_t)_i = \frac{\|\tilde{G}_{t,:;i}^O\|}{\|\tilde{G}_{t,:;i}\|} \quad (11)$$

As suggested by Fira [Chen et al., 2025], this additional term must be controlled using a gradient-clipping-like method to ensure training stability. Building on their observation, we also limit the growth rate of $\Lambda_t = \phi_t(G_t)(G_t - S_t \hat{G}_t)$ by a factor ζ , and apply a correction whenever it exceeds this threshold as:

$$\Lambda_t \leftarrow \frac{\Lambda_t}{\|\Lambda_t\|} \cdot \zeta \|\Lambda_{t-1}\| \quad (12)$$

By incorporating a geometry-aware perspective into low-rank optimization and applying this approach across all components of the training pipeline, SubTrack++ demonstrates robust and stable training, and achieves state-of-the-art performance while maintaining minimal memory footprint and wall-time. The overall flow of operations in SubTrack++ is illustrated in Algorithm 1.

3 Theoretical Analysis

In this section, we analyze the convergence of Grassmannian Subspace Tracking applied in SubTrack++ using theoretical analysis. To begin, the general weights update rule is as follows:

$$W_t = W_0 - \alpha \cdot \sum_{t'=0}^{t-1} \hat{G}_{t'} \quad (13)$$

As previously mentioned, we use left projection if $m \leq n$, where m and n are the dimensions of the gradient matrix, and vice versa. Thus, $\hat{G}_{t'}$ can be computed as shown in (14).

$$\hat{G}_{t'} = \begin{cases} S_{t'} \rho_{t'} (S_{t'}^\top G_{t'}), & \text{if } m \leq n \\ \rho_{t'} (G_{t'} S_{t'}^\top) S_{t'}^\top, & \text{otherwise} \end{cases} \quad (14)$$

Here, $S_{t'}$ is the projection matrix that projects the gradient onto the subspace, and $\rho_{t'}$ is representing the entry-wise regularizer used in the optimizer. If we use the full projection, then $\hat{G}_{t'}$ will be computed as shown in (15); where $S_{t'}^l$ and $S_{t'}^r$ are the rank- r left and right projection matrices.

$$\hat{G}_{t'} = S_{t'}^l \rho_{t'} (S_{t'}^{l\top} G_{t'} S_{t'}^r) S_{t'}^{r\top} \quad (15)$$

Definition 3.1 (L-continuity). A function $f(X)$ has Lipschitz-continuity (L-continuity) if for any X_1 and X_2 , $\|f(X_2) - f(X_1)\|_F \leq L \|X_2 - X_1\|_F$

Theorem 3.2 (Convergence of Grassmannian Subspace Tracking). *Suppose gradient has the following form with functions A_i , B_i , and C_i being L-continuous as per Def. 3.1 with constants L_A , L_B , and L_C w.r.t. weight matrix W_t ; and $\|W_t\|_F \leq M$; where W_t denotes the weight matrix at step t , and M is a scalar value,*

$$G = \sum_i A_i + \sum_i B_i W C_i.$$

Now, define $\widehat{B}_{i,t} = (S_{i,t}^l)^\top B_i(W_t) S_{i,t}^l$ and $\widehat{C}_{i,t} = (S_{i,t}^r)^\top C_i(W_t) S_{i,t}^r$, where $S_{i,t}^l$ and $S_{i,t}^r$ are the rank- r left and right projection matrices; $B_i(W_t)$ and $C_i(W_t)$ denote the dependence of B_i and C_i on the weight matrices W_t . Further letting $P_t = S_t^l{}^\top G_t S_t^r$, and $\kappa_t = \frac{1}{N} \sum_i \lambda_{\min}(\widehat{B}_{i,t}) \lambda_{\min}(\widehat{C}_{i,t})$, where $\lambda_{\min}(\cdot)$ denotes the minimum eigenvalue over each batch, and N representing the number of samples in a batch. Assuming that the projection matrices remain constant during the training. Then for learning-rate μ and $\min(\kappa_t) > (L_A + 2L_B L_C M^2)$, subspace tracking, with $\rho_t \equiv 1$ (the element-wise regularizer of the optimizer) satisfies:

$$\|P_t\|_F \leq [1 - \mu(\kappa_{t-1} - L_A - 2L_B L_C M^2)] \|P_{t-1}\|_F.$$

That is, $P_t \rightarrow 0$ and it converges.

The proof of Theorem 3.2 is provided in Appendix A, based on Zhao et al. [2024]. While both GaLore and SubTrack++ assume the subspace remains unchanged for the proof of convergence, GaLore must limit these updates to ensure convergence, as each update can potentially change the entire subspace. In contrast, SubTrack++ leverages rank-1 updates to the subspace, preventing drastic changes with each update. While a deeper analysis of slowly changing subspaces and their impact on convergence remains an open problem, in practice, this allows SubTrack++ to perform more frequent updates.

Here we investigate the Grassmannian update rule presented in (5), which is a direct application of Grassmann geometry [Edelman et al., 1998, Bendokat et al., 2024].

Definition 3.3 (Exponential Map). The exponential map $\exp_p : T_p M \rightarrow M$ on a Riemannian manifold M is a mapping that assigns the point $\gamma(1) \in M$ to each tangent vector $\Delta \in T_p M$, where $T_p M$ is the tangent space of M at p , and γ is the unique geodesic originating at p with initial velocity Δ . This map establishes a relationship between geodesics and the Riemannian exponential, such that $\gamma(t) = \exp_p(t\Delta)$ for $t \in \mathbb{R}$.

Definition 3.4 (Stiefel Manifold). The Stiefel manifold $St(n, p)$, parametrizes the set of all $n \times p$ orthonormal matrices U , each representing a rank- p subspace of \mathbb{R}^n .

Definition 3.5 (Grassmann Manifold). The Grassmannian manifold $Gr(n, p)$ parametrizes the set of all p -dimensional subspaces of \mathbb{R}^n . Each point can be represented by a projection matrix $P = UU^\top$, where $U \in St(n, p)$.

Theorem 3.6 (Grassmann Exponential). Let $P = UU^\top \in Gr(n, p)$ be a point on the Grassmannian, where $U \in St(n, p)$ is the orthonormal basis of the corresponding subspace. Consider a tangent vector $\Delta \in T_P Gr(n, p)$, and let Δ_U^{hor} denote the horizontal lift of Δ to the horizontal space at U in the Stiefel manifold $St(n, p)$. Suppose the thin SVD of Δ_U^{hor} is given by $\Delta_U^{hor} = \hat{Q} \Sigma V^\top$, where $\hat{Q} \in St(n, r)$, $\Sigma = \text{diag}(\sigma_1, \dots, \sigma_r)$ contains the nonzero singular values of Δ_U^{hor} with $r = \min(p, n - p)$, and $V \in St(p, r)$. The Grassmann exponential map, representing the geodesic emanating from P in the direction Δ , is given by:

$$\text{Exp}_P^{Gr}(t\Delta) = [UV \cos(t\Sigma) V^\top + \hat{Q} \sin(t\Sigma) V^\top + UV_\perp V_\perp^\top],$$

where $V_\perp \in \mathbb{R}^{p \times (p-r)}$ is any orthogonal complement of V .

The proof of Theorem 3.6 can be found in Appendix B. Leveraging this theorem and our notation in section 2, one can easily verify that the subspace update rule is as follows:

$$S_{t+1}(\eta) = (S_t \widehat{V}_F \quad \widehat{U}_F) \begin{pmatrix} \cos \widehat{\Sigma}_F \eta \\ \sin \widehat{\Sigma}_F \eta \end{pmatrix} \widehat{V}_F^\top + S_t (I - \widehat{V}_F \widehat{V}_F^\top)$$

This update rule generally converges to a stable subspace if the step size η decreases over time [Balzano et al., 2011]. However, a decreasing step size can impair the ability to accurately track and adapt to subspace changes. Consequently, SubTrack++ uses a constant step size to effectively adjust subspaces. This approach does not hinder convergence, as proved in Theorem 3.2, which guarantees convergence as long as changes are controlled to maintain the stable subspace assumption.

4 Experiments and Results

To ensure fair comparison, we evaluated SubTrack++ across diverse models and datasets through pre-training and fine-tuning, measuring key metrics critical to LLM democratization.

Table 1: We compare evaluation loss for pre-training Llama-based architectures on the C4 dataset over 10K iterations. SubTrack++ outperforms all other baselines in nearly every configuration. The best results are marked in **bold**, with the second-best performance underlined. *LDAdam could not be run on the 7B configuration due to an out-of-memory error with our available resources.

	60M r=128	130M r=256	350M r=256	1B r=512	3B r=512	7B r=1024
Full-Rank	3.41	3.25	3.40	4.61	4.52	4.30
GaLore [Zhao et al., 2024]	4.02	3.61	3.62	6.53	6.57	<u>5.55</u>
BAdam [Luo et al., 2024]	7.86	7.08	7.62	7.28	7.12	6.76
Online Subspace Descent [Liang et al., 2024]	4.18	3.88	4.09	6.79	6.85	5.69
LDAdam [Robert et al., 2025]	<u>3.52</u>	<u>3.44</u>	<u>3.67</u>	<u>4.70</u>	4.39	OOM*
Fira [Chen et al., 2025]	3.80	3.55	3.56	6.31	6.50	6.83
SubTrack++ (Ours)	3.43	3.24	3.29	4.51	<u>4.49</u>	4.62

Pre-Training Experiments. We pre-trained several Llama-based models on the C4 dataset, with results in Table 1. To ensure a fair comparison, we benchmarked against a diverse set of baselines. BAdam [Luo et al., 2024] is notably efficient in both memory and time, but its reliance on partial parameter updates leads to reduced performance. GaLore [Zhao et al., 2024] supports full-parameter training with low memory usage, though this comes at the cost of more than 150% increase in wall-time relative to AdamW in large models. As another relative baseline, Online Subspace Descent [Liang et al., 2024] uses Online PCA to track gradient subspace. LDAdam [Robert et al., 2025] and Fira [Chen et al., 2025] deliver strong performance at the cost of increasing wall-time even more than GaLore. Across these methods, SubTrack++ achieves SOTA results while using 14% less memory and running 43% faster than LDAdam, the most accurate baseline on 1B model. Hyperparameter details are provided in Appendix G, with a detailed wall-time and memory analysis in Appendix F.

Figure 4 compares pre-training performance of a 1B-parameter Llama model across several baselines. SubTrack++ converges fastest in both steps and wall-time, emphasizing the power of geometry-aware optimization in boosting performance, reducing resource demands, and democratizing access to SOTA training methods.

Ablation Study. We conducted an ablation study to evaluate the individual and combined effects of projection-aware optimizers and recovery scaling, integrated with Grassmannian subspace tracking on the 1B Llama model. We use the experimental settings outlined in Table 10. As shown in Figure 3, projection-aware optimizer and recovery scaling independently yield substantial improvements over pure Grassmannian subspace tracking, reducing loss from 6.53 to 5.43 and 5.28, respectively; while their combination, SubTrack++ , achieves 4.51 surpassing all baselines. Notably, these gains are achieved with minimal increases in runtime and memory.

Fine-Tuning Experiments. RoBERTa-Base and RoBERTa-Large are fine-tuned on GLUE and SuperGLUE tasks; with the results presented in Table 4 and 5, respectively. More details and hyperparameters are provided in Appendix E.

Time and Space Complexity. Table 2 provides memory requirements of the optimizer states and the time complexity of the subspace update step considering an $m \times n$ gradient matrix with $m \leq n$. GaLore [Zhao et al., 2024] and Fira [Chen et al., 2025] periodically perform SVD to estimate the underlying subspace, while LDAdam [Robert et al., 2025] relies on the faster PowerSGD to update the

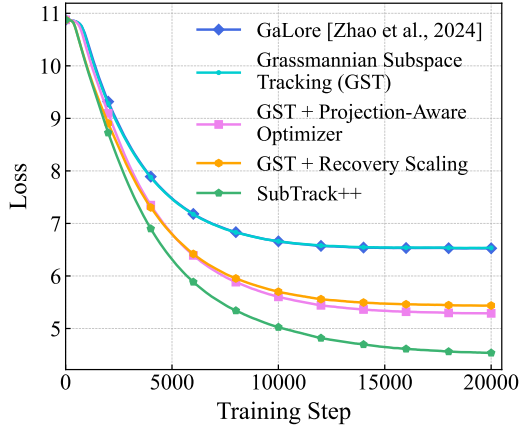


Figure 3: Ablation study comparing pure Grassmannian subspace tracking with incremental additions of the projection-aware optimizer and recovery scaling, leading to SubTrack++ . While Grassmannian tracking alone matches GaLore’s step-wise convergence, it significantly reduces wall-time, as shown in Figure 4.

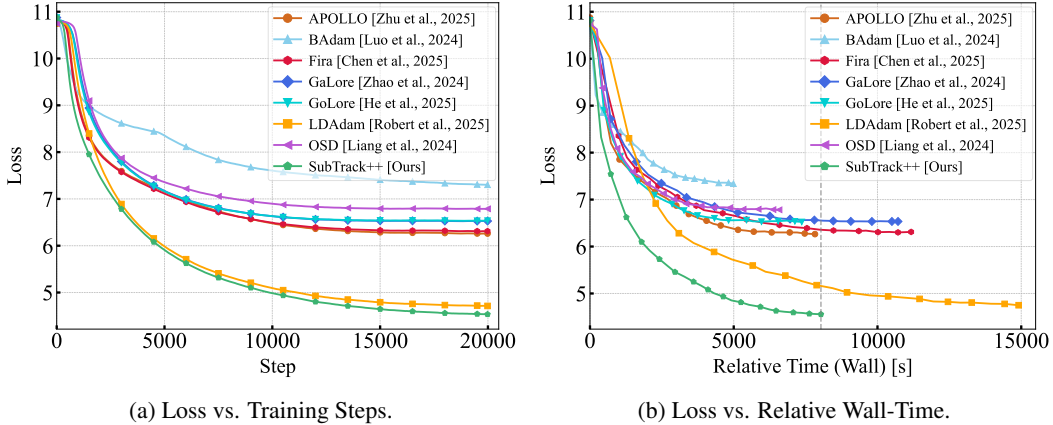


Figure 4: We compare several baselines in pre-training a 1B parameter model. (a) shows training loss versus training steps. (b) shows the same runs against wall-time. SubTrack++ consistently outperforms all baselines, achieving the lowest loss in the shortest wall-time; substantially reducing wall-time compared to LDAdam, the top-performing baseline.

subspace at every iteration. In contrast, SubTrack++ employs Grassmannian-based subspace tracking at the same frequency as GaLore and Fira. Comparing the time complexities of these methods, highlights why SubTrack++ is significantly more efficient than SVD-based methods. A breakdown of the subspace update time complexity for SubTrack++ is shown in Appendix D. Additionally, the memory required for storing optimizer states in SubTrack++ , is equivalent to GaLore and other baselines.

Robust Subspace Tracking. Relying on SVD for subspace updates makes methods sensitive to noise and abrupt changes [He et al., 2025]. Figure 5 compares Grassmannian subspace tracking with GaLore’s SVD on the Ackley function, highlighting how SVD causes erratic jumps, while our subspace tracking ensures robust optimization. GaLore struggles to reach the global minimum within 100 steps at scale factor 1, and although increasing the scale factor to 3 improves performance, it amplifies jumps that hinder convergence in non-convex settings, revealing sensitivity to hyperparameters, noise, and abrupt changes.

Table 2: The optimizer’s state parameter count and subspace update time complexity across baselines, given a gradient matrix of dimension $m \times n$ and projection rank r where $r \ll m \leq n$. *LDAdam updates the subspace at every iteration, while other methods update it every k steps.

	Optimizer Mem.	Subspace Update Time
Adam	$2mn$	–
LDAdam*	$mr + 2nr$	$O(mnr)$
GaLore, Fira	$mr + 2nr$	$O(nm^2)$
SubTrack++	$mr + 2nr$	$O(mnr)$

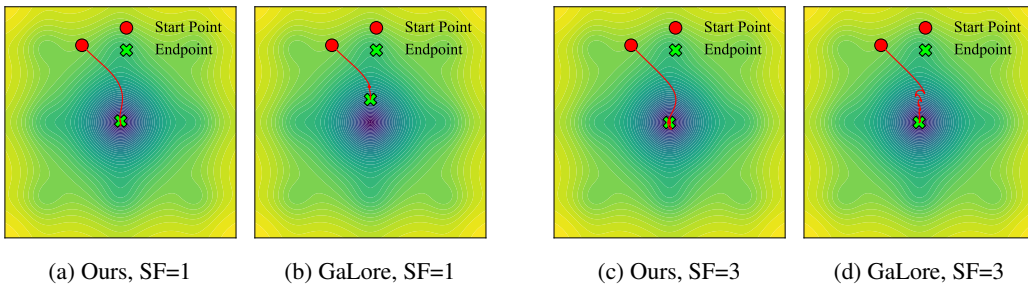


Figure 5: Comparison of Grassmannian subspace tracking (Ours) (a, c) and GaLore’s SVD (b, d) on the Ackley Function over 100 optimization steps, with a subspace update interval of 10. SF stands for scale factor; with a scale factor of 1, GaLore fails to reach the global minimum due to abrupt jumps. At a scale factor of 3, while the minimum is reached, the jump length increases. This demonstrates SVD’s sensitivity to noise and abrupt changes, highlighting the robustness of our Subspace Tracking method with its controlled subspace updates.

5 Related Works

Parameter-Efficient Training. Several works aim to improve the efficiency of training LLMs, addressing a growing demand as their popularity rapidly increases. Popular LoRA [Hu et al., 2021] significantly reduces memory requirements for fine-tuning LLMs by leveraging two low-rank trainable low-rank matrices. Dettmers et al. [2024] employ quantization techniques and paged optimizers to further reduce memory usage. Additionally, Yaras et al. [2024] introduce Deep LoRA to address overfitting issues and reducing the need for precise tuning of the rank parameter. Several other works have also extended LoRA to enhance the efficiency of training and fine-tuning LLMs [Lialin et al., 2023, Renduchintala et al., 2024, Xia et al., 2024, Pan et al., 2024]. Miles et al. [2024] propose compressing intermediate activations and reconstructing them during backpropagation to enhance memory efficiency. Additionally, Hao et al. [2024] demonstrate that full-parameter fine-tuning is feasible by random projections on the gradient matrix, showing that LoRA essentially performs a down-projection of the gradient. BAdam [Luo et al., 2024] leverages the block coordinate descent framework to reduce memory consumption while maintaining capabilities comparable to Adam.

Gradient Low-Rank Projection. Several approaches aim to reduce optimizer states, as optimizers like Adam [Kingma and Ba, 2017] account for a significant portion of memory footprint [Li et al., 2023, Anil et al., 2019, Lv et al., 2024, Dettmers et al., 2022]. MicroAdam [Modoranu et al., 2024] tackles this by compressing the gradient space and utilizing the compression error through feedback loops. Adam-mini [Zhang et al., 2024] partitions model into blocks, assigning a single learning rate to each block to preserve performance while saving memory. Gur-Ari et al. [2018], Schneider et al. [2024], Yaras et al. [2023] suggest that a substantial portion of gradients lies within a largely consistent subspace. GaLore [Zhao et al., 2024] leverages this fact to reduce the optimizer’s memory by projecting gradients into a low-rank subspace and then projecting them back for full parameter tuning. This approach has been integrated with other methods regarding efficient LLM training [Li et al., 2024, Rajabi and Rambhatla, 2024b]. However, not all layers’ gradients evolve within a stable low-rank subspace. Jaiswal et al. [2024], Rajabi and Rambhatla [2024d] identify layers where gradients evolve within a low-dimensional subspace and fine-tune only those layers, freezing the others to avoid inefficient low-rank updates. Grass [Muhamed et al., 2024] reduces memory usage by applying sparse projection matrices to the gradient. Ramesh et al. [2024] dynamically select and update a subset of parameters, for a fast and memory-efficient training. FIRA [Chen et al., 2025] utilize a norm-based scaling method along with GaLore to maintain performance comparable to full-rank training. GoLore [He et al., 2025] addresses GaLore’s convergence issues and employ random projection in latter steps as a solutions. LDAdam [Robert et al., 2025] performs optimization within lower-dimensional subspaces, incorporating a projection-aware optimization update rule and a generalized error feedback mechanism. APOLLO [Zhu et al., 2025] approximates channel-wise learning rate scaling based on random projection. Also, Liang et al. [2024] introduce a dynamically evolving projection matrix updated via online PCA, enhancing the model’s ability to navigate the parameter space efficiently without relying on expensive SVD, a similar approach is also proposed in Rajabi and Rambhatla [2024a].

Grassmannian and Subspace Tracking. A common approach in working with high-dimensional data is to project the data into a lower-dimensional space, and many studies focus on tracking these subspaces as they evolve. Balzano et al. [2011], Rajabi and Rambhatla [2024c] introduce an incremental method for updating subspaces on the Grassmannian when the data is partially observed. Zhang and Balzano [2016] and Kasai [2017] propose methods to handle noise effect in tracking these subspaces. Furthermore, Blocker et al. [2023] present a method for evolving geodesic-based data in the Grassmannian for updating the subspace effectively.

6 Discussion and Conclusion

We propose SubTrack++ , a time- and memory-efficient approach that projects gradients into a low-rank subspace and uses Grassmannian subspace tracking to preserve the computed subspace while incorporating gradient components from the orthogonal complement. By integrating projection-aware optimizers that reflect subspace changes in Adam’s internal statistics and utilizing the gradient information lost during low-rank projection, SubTrack++ achieves state-of-the-art convergence and accuracy across all baselines. While Grassmannian subspace tracking integrates seamlessly with various optimizers as a plug-and-play module, extending projection-aware optimization beyond the

Adam family requires further design and investigation. Also benchmarking on models with more than 7B parameters was not feasible regarding our limited time and resources.

References

- Jiawei Zhao, Zhenyu Zhang, Beidi Chen, Zhangyang Wang, Anima Anandkumar, and Yuandong Tian. Galore: Memory-efficient llm training by gradient low-rank projection, 2024. URL <https://arxiv.org/abs/2403.03507>.
- Ajay Jaiswal, Lu Yin, Zhenyu Zhang, Shiwei Liu, Jiawei Zhao, Yuandong Tian, and Zhangyang Wang. From galore to welore: How low-rank weights non-uniformly emerge from low-rank gradients, 2024. URL <https://arxiv.org/abs/2407.11239>.
- Aashiq Muhamed, Oscar Li, David Woodruff, Mona Diab, and Virginia Smith. Grass: Compute efficient low-memory llm training with structured sparse gradients, 2024. URL <https://arxiv.org/abs/2406.17660>.
- Roy Miles, Pradyumna Reddy, Ismail Elezi, and Jiankang Deng. Velora: Memory efficient training using rank-1 sub-token projections, 2024. URL <https://arxiv.org/abs/2405.17991>.
- Ionut-Vlad Modoranu, Mher Safaryan, Grigory Malinovsky, Eldar Kurtic, Thomas Robert, Peter Richtarik, and Dan Alistarh. Microadam: Accurate adaptive optimization with low space overhead and provable convergence, 2024. URL <https://arxiv.org/abs/2405.15593>.
- Yongchang Hao, Yanshuai Cao, and Lili Mou. Flora: Low-rank adapters are secretly gradient compressors, 2024. URL <https://arxiv.org/abs/2402.03293>.
- Pengxiang Li, Lu Yin, Xiaowei Gao, and Shiwei Liu. Owlora: Outlier-weighted layerwise sampled low-rank projection for memory-efficient llm fine-tuning, 2024. URL <https://arxiv.org/abs/2405.18380>.
- Tianqi Chen, Bing Xu, Chiyuan Zhang, and Carlos Guestrin. Training deep nets with sublinear memory cost, 2016. URL <https://arxiv.org/abs/1604.06174>.
- Samyam Rajbhandari, Jeff Rasley, Olatunji Ruwase, and Yuxiong He. Zero: Memory optimizations toward training trillion parameter models, 2020. URL <https://arxiv.org/abs/1910.02054>.
- Edward J Hu, Yelong Shen, Phillip Wallis, Zeyuan Allen-Zhu, Yuanzhi Li, Shean Wang, Lu Wang, and Weizhu Chen. Lora: Low-rank adaptation of large language models. *arXiv preprint arXiv:2106.09685*, 2021.
- Tim Dettmers, Artidoro Pagnoni, Ari Holtzman, and Luke Zettlemoyer. Qlora: Efficient finetuning of quantized llms. *Advances in Neural Information Processing Systems*, 36, 2024.
- Can Yaras, Peng Wang, Laura Balzano, and Qing Qu. Compressible dynamics in deep overparameterized low-rank learning & adaptation. *arXiv preprint arXiv:2406.04112*, 2024.
- Vladislav Lialin, Namrata Shivagunde, Sherin Muckatira, and Anna Rumshisky. Relora: High-rank training through low-rank updates, 2023. URL <https://arxiv.org/abs/2307.05695>.
- Adithya Renduchintala, Tugrul Konuk, and Oleksii Kuchaiev. Tied-LoRA: Enhancing parameter efficiency of LoRA with weight tying. In Kevin Duh, Helena Gomez, and Steven Bethard, editors, *Proceedings of the 2024 Conference of the North American Chapter of the Association for Computational Linguistics: Human Language Technologies (Volume 1: Long Papers)*, pages 8694–8705, Mexico City, Mexico, June 2024. Association for Computational Linguistics. doi: 10.18653/v1/2024.naacl-long.481. URL <https://aclanthology.org/2024.naacl-long.481>.
- Wenhan Xia, Chengwei Qin, and Elad Hazan. Chain of lora: Efficient fine-tuning of language models via residual learning, 2024. URL <https://arxiv.org/abs/2401.04151>.
- Qijun Luo, Hengxu Yu, and Xiao Li. Badam: A memory efficient full parameter optimization method for large language models, 2024. URL <https://arxiv.org/abs/2404.02827>.

- Amrutha Varshini Ramesh, Vignesh Ganapathiraman, Issam H. Laradji, and Mark Schmidt. Blockllm: Memory-efficient adaptation of llms by selecting and optimizing the right coordinate blocks, 2024. URL <https://arxiv.org/abs/2406.17296>.
- Bingrui Li, Jianfei Chen, and Jun Zhu. Memory efficient optimizers with 4-bit states, 2023. URL <https://arxiv.org/abs/2309.01507>.
- Rohan Anil, Vineet Gupta, Tomer Koren, and Yoram Singer. Memory-efficient adaptive optimization, 2019. URL <https://arxiv.org/abs/1901.11150>.
- Kai Lv, Yuqing Yang, Tengxiao Liu, Qipeng Guo, and Xipeng Qiu. Full parameter fine-tuning for large language models with limited resources. In Lun-Wei Ku, Andre Martins, and Vivek Srikumar, editors, *Proceedings of the 62nd Annual Meeting of the Association for Computational Linguistics (Volume 1: Long Papers)*, pages 8187–8198, Bangkok, Thailand, August 2024. Association for Computational Linguistics. URL <https://aclanthology.org/2024.acl-long.445>.
- Tim Dettmers, Mike Lewis, Sam Shleifer, and Luke Zettlemoyer. 8-bit optimizers via block-wise quantization, 2022. URL <https://arxiv.org/abs/2110.02861>.
- Yushun Zhang, Congliang Chen, Ziniu Li, Tian Ding, Chenwei Wu, Yinyu Ye, Zhi-Quan Luo, and Ruoyu Sun. Adam-mini: Use fewer learning rates to gain more, 2024. URL <https://arxiv.org/abs/2406.16793>.
- Sahar Rajabi and Sirisha Rambhatla. Accelerating memory-efficient llm training and fine-tuning via tracking the gradient subspace. In *Workshop on Machine Learning and Compression, NeurIPS 2024*, 2024a.
- Guy Gur-Ari, Daniel A. Roberts, and Ethan Dyer. Gradient descent happens in a tiny subspace, 2018. URL <https://arxiv.org/abs/1812.04754>.
- Jan Schneider, Pierre Schumacher, Simon Guist, Le Chen, Daniel Häufle, Bernhard Schölkopf, and Dieter Büchler. Identifying policy gradient subspaces, 2024. URL <https://arxiv.org/abs/2401.06604>.
- Can Yaras, Peng Wang, Wei Hu, Zhihui Zhu, Laura Balzano, and Qing Qu. Invariant low-dimensional subspaces in gradient descent for learning deep matrix factorizations. In *NeurIPS 2023 Workshop on Mathematics of Modern Machine Learning*, 2023.
- Xi Chen, Kaituo Feng, Changsheng Li, Xunhao Lai, Xiangyu Yue, Ye Yuan, and Guoren Wang. Fira: Can we achieve full-rank training of LLMs under low-rank constraint?, 2025. URL <https://openreview.net/forum?id=1R7rqLtsXZ>.
- Thomas Robert, Mher Safaryan, Ionut-Vlad Modoranu, and Dan Alistarh. LDAdam: Adaptive optimization from low-dimensional gradient statistics. In *The Thirteenth International Conference on Learning Representations*, 2025. URL <https://openreview.net/forum?id=Zkp1GuHerF>.
- Hanqing Zhu, Zhenyu Zhang, Wenyan Cong, Xi Liu, Sem Park, Vikas Chandra, Bo Long, David Z. Pan, Zhangyang Wang, and Jinwon Lee. Apollo: Sgd-like memory, adamw-level performance, 2025. URL <https://arxiv.org/abs/2412.05270>.
- Yutong He, Pengrui Li, Yipeng Hu, Chuyan Chen, and Kun Yuan. Subspace optimization for large language models with convergence guarantees, 2025. URL <https://openreview.net/forum?id=udtrtwkvk5>.
- Kaizhao Liang, Bo Liu, Lizhang Chen, and qiang liu. Memory-efficient LLM training with online subspace descent. In *The Thirty-eighth Annual Conference on Neural Information Processing Systems*, 2024. URL <https://openreview.net/forum?id=P8rTCT6g45>.
- Sahar Rajabi and Sirisha Rambhatla. Memory-efficient large language model (llm) training and fine-tuning via gradient subspace tracking. In *OPT 2024: Optimization for Machine Learning*, 2024b.

- Namrata Vaswani, Thierry Bouwmans, Sajid Javed, and Praneeth Narayanamurthy. Robust subspace learning: Robust pca, robust subspace tracking, and robust subspace recovery. *IEEE Signal Processing Magazine*, 35(4):32–55, July 2018. ISSN 1558-0792. doi: 10.1109/msp.2018.2826566. URL <http://dx.doi.org/10.1109/MSP.2018.2826566>.
- Jiayao Zhang, Guangxu Zhu, Robert W Heath Jr, and Kaibin Huang. Grassmannian learning: Embedding geometry awareness in shallow and deep learning. *arXiv preprint arXiv:1808.02229*, 2018.
- Laura Balzano, Robert Nowak, and Benjamin Recht. Online identification and tracking of subspaces from highly incomplete information, 2011. URL <https://arxiv.org/abs/1006.4046>.
- Jun He, Laura Balzano, and John C. S. Lui. Online robust subspace tracking from partial information, 2011. URL <https://arxiv.org/abs/1109.3827>.
- Sahar Rajabi and Sirisha Rambhatla. Optimizing fine-tuning efficiency: Gradient subspace tracking on grassmann manifolds for large language models. In *NeurIPS 2024 Workshop on Mathematics of Modern Machine Learning*, 2024c.
- Cameron J. Blocker, Haroon Raja, Jeffrey A. Fessler, and Laura Balzano. Dynamic subspace estimation with grassmannian geodesics, 2023. URL <https://arxiv.org/abs/2303.14851>.
- Rudransh Chakraborty, Søren Hauberg, and Baba C. Vemuri. Intrinsic grassmann averages for online linear and robust subspace learning. In *2017 IEEE Conference on Computer Vision and Pattern Recognition (CVPR)*, pages 801–809, 2017. doi: 10.1109/CVPR.2017.92.
- Dejjiao Zhang and Laura Balzano. Global convergence of a grassmannian gradient descent algorithm for subspace estimation, 2016. URL <https://arxiv.org/abs/1506.07405>.
- Laura Balzano, Yuejie Chi, and Yue M Lu. Streaming pca and subspace tracking: The missing data case. *Proceedings of the IEEE*, 106(8):1293–1310, 2018.
- Yongmin Li. On incremental and robust subspace learning. *Pattern recognition*, 37(7):1509–1518, 2004.
- Laura Kathryn Balzano. *Handling missing data in high-dimensional subspace modeling*. PhD thesis, The University of Wisconsin-Madison, 2012.
- Thomas Bendokat, Ralf Zimmermann, and P.-A. Absil. A grassmann manifold handbook: basic geometry and computational aspects. *Advances in Computational Mathematics*, 50(1), January 2024. ISSN 1572-9044. doi: 10.1007/s10444-023-10090-8. URL <http://dx.doi.org/10.1007/s10444-023-10090-8>.
- Alan Edelman, T. A. Arias, and Steven T. Smith. The geometry of algorithms with orthogonality constraints, 1998. URL <https://arxiv.org/abs/physics/9806030>.
- Rui Pan, Xiang Liu, Shizhe Diao, Renjie Pi, Jipeng Zhang, Chi Han, and Tong Zhang. Lisa: Layerwise importance sampling for memory-efficient large language model fine-tuning, 2024. URL <https://arxiv.org/abs/2403.17919>.
- Diederik P. Kingma and Jimmy Ba. Adam: A method for stochastic optimization, 2017. URL <https://arxiv.org/abs/1412.6980>.
- Sahar Rajabi and Sirisha Rambhatla. Enhancing fine-tuning efficiency of llms through gradient subspace tracking. In *Adaptive Foundation Models: Evolving AI for Personalized and Efficient Learning*, 2024d.
- Hiroyuki Kasai. Fast online low-rank tensor subspace tracking by cp decomposition using recursive least squares from incomplete observations, 2017. URL <https://arxiv.org/abs/1709.10276>.

A Convergence of SubTrack++

Theorem 3.2 (Convergence of Grassmannian Subspace Tracking). *Suppose gradient has the following form with functions A_i , B_i , and C_i being L -continuous as per [Def. 3.1](#) with constants L_A , L_B , and L_C w.r.t. weight matrix W_t ; and $\|W_t\|_F \leq M$; where W_t denotes the weight matrix at step t , and M is a scalar value,*

$$G = \sum_i A_i + \sum_i B_i W C_i.$$

Now, define $\widehat{B}_{i,t} = (S_{i,t}^l)^\top B_i(W_t) S_{i,t}^l$ and $\widehat{C}_{i,t} = (S_{i,t}^r)^\top C_i(W_t) S_{i,t}^r$, where $S_{i,t}^l$ and $S_{i,t}^r$ are the rank- r left and right projection matrices; $B_i(W_t)$ and $C_i(W_t)$ denote the dependence of B_i and C_i on the weight matrices W_t . Further letting $P_t = S_t^{l\top} G_t S_t^r$, and $\kappa_t = \frac{1}{N} \sum_i \lambda_{\min}(\widehat{B}_{i,t}) \lambda_{\min}(\widehat{C}_{i,t})$, where $\lambda_{\min}(\cdot)$ denotes the minimum eigenvalue over each batch, and N representing the number of samples in a batch. Assuming that the projection matrices remain constant during the training. Then for learning-rate μ and $\min(\kappa_t) > (L_A + 2L_B L_C M^2)$, subspace tracking, with $\rho_t \equiv 1$ (the element-wise regularizer of the optimizer) satisfies:

$$\|P_t\|_F \leq [1 - \mu(\kappa_{t-1} - L_A - 2L_B L_C M^2)] \|P_{t-1}\|_F.$$

That is, $P_t \rightarrow 0$ and it converges.

proof. To demonstrate that SubTrack++ converges to the global minimum during training, we begin by deriving the recursive form of the gradients.

Let \otimes denote the Kronecker product. Then, $\text{vec}(AXB) = (B^\top \otimes A) \text{vec}(X)$.

By applying vec to the gradient form given in the theorem, we obtain:

$$g_t = \text{vec}(G_t) = \text{vec}\left(\sum_i A_i + \sum_i B_i W C_i\right) = a_t - D_t w_t \quad (16)$$

where $g_t := \text{vec}(G_t)$, $w_t := \text{vec}(W_t)$, $a_t := \frac{1}{N} \sum_i \text{vec}(A_{i,t})$, and $D_t = \frac{1}{N} \sum_i C_{i,t} \otimes B_{i,t}$.

As defined in the theorem, let $P_t = S_t^{l\top} G_t S_t^r$. Its vectorized form can be expressed using the Kronecker product as follows:

$$\begin{aligned} p_t = \text{vec}(P_t) &= \text{vec}(S_t^{l\top} G_t S_t^r) = (S_t^{r\top} \otimes S_t^{l\top}) \text{vec}(G_t) \\ &= (S_t^r \otimes S_t^l)^\top \text{vec}(G_t) = (S_t^r \otimes S_t^l)^\top g_t \end{aligned} \quad (17)$$

Now recalling \widehat{G}_t from (15), it can be written as:

$$\widehat{G}_t = S_t^l S_t^{l\top} G_t S_t^r S_t^{r\top}$$

Thus, its vectorized form will be:

$$\begin{aligned} \text{vec}(\widehat{G}_t) = \widehat{g}_t &= \text{vec}(S_t^l S_t^{l\top} G_t S_t^r S_t^{r\top}) = \text{vec}(S_t^l P_t S_t^{r\top}) \\ &= (S_t^r \otimes S_t^l) \text{vec}(P_t) = (S_t^r \otimes S_t^l) p_t \end{aligned} \quad (18)$$

This is where the constant subspace assumption becomes necessary. To derive the recursive form of g_t , we assume that the projection matrices remain fixed throughout training, i.e., $S_t^r = S^r$ and $S_t^l = S^l$. Consequently, we can restate equations (17) and (18) as follows:

$$p_t = (S^r \otimes S^l)^\top g_t \quad (19)$$

$$\widehat{g}_t = (S^r \otimes S^l) p_t \quad (20)$$

Then we can write the recursive form of g_t :

$$\begin{aligned} g_t = a_t - D_t w_t &= (a_t - a_{t-1}) + (D_{t-1} - D_t) w_t + a_{t-1} - D_{t-1} w_t \\ &= e_t + a_{t-1} - D_{t-1} (w_{t-1} + \mu \widehat{g}_{t-1}) = e_t + g_{t-1} - \mu D_{t-1} \widehat{g}_{t-1} \end{aligned} \quad (21)$$

where $e_t := (a_t - a_{t-1}) + (D_{t-1} - D_t) w_t$.

Note that in deriving (21), we utilized the general form of the weight update rule, $w_{t+1} = w_t - \mu g_t$, which can be rewritten as $w_t = w_{t+1} + \mu g_t$. By applying this rule along with (16), we arrive at the second equality in (21) as follows:

$$\begin{aligned}
g_t &= a_t - D_t w_t = a_t - D_t w_t - g_{t-1} + g_{t-1} \\
&= a_t - D_t w_t - a_{t-1} + D_{t-1} w_{t-1} + a_{t-1} - D_{t-1} w_{t-1} \\
&= a_t - D_t w_t - a_{t-1} + D_{t-1} (w_t + \mu g_{t-1}) + a_{t-1} - D_{t-1} (w_t + \mu g_{t-1}) \\
&= a_t - D_t w_t - a_{t-1} + D_{t-1} w_t + \mu D_{t-1} g_{t-1} + a_{t-1} - D_{t-1} w_t - \mu D_{t-1} g_{t-1} \\
&= a_t - a_{t-1} + (D_{t-1} - D_t) w_t + a_{t-1} - D_{t-1}
\end{aligned}$$

To obtain p_t from this recursive formulation, we can left-multiply by $(S^r \otimes S^l)^\top$, as shown in (20):

$$p_t = (S^r \otimes S^l)^\top e_t + (S^r \otimes S^l)^\top g_{t-1} - \mu (S^r \otimes S^l)^\top D_{t-1} \hat{g}_{t-1} \quad (22)$$

Now, based on (19) and (20), p_t can be written as:

$$p_t = (S^r \otimes S^l)^\top e_t + p_{t-1} - \mu (S^r \otimes S^l)^\top D_{t-1} (S^r \otimes S^l) p_{t-1} \quad (23)$$

Let define:

$$\begin{aligned}
\hat{D}_t &:= (S^r \otimes S^l)^\top D_t (S^r \otimes S^l) = \frac{1}{N} \sum_i (S^r \otimes S^l)^\top (C_{i,t} \otimes B_{i,t}) (S^r \otimes S^l) \\
&= \frac{1}{N} \sum_i (S^{r\top} C_{i,t} S^r) \otimes (S^{l\top} B_{i,t} S^l)
\end{aligned} \quad (24)$$

Then we can expand (23) and show that:

$$p_t = (I - \mu \hat{D}_{t-1}) p_{t-1} + (S^r \otimes S^l)^\top e_t \quad (25)$$

Note that S^l and S^r are orthonormal matrices. This is ensured because the subspace is initialized using the SVD of G_0 , and the Grassmannian update rule provided in (5) preserves the orthonormality of the subspace matrices throughout training. Since S^l and S^r are orthonormal, we have $S^{l\top} S^l = I$ and $S^{r\top} S^r = I$. Consequently, we can bound the norm of the second term in (25) as follows:

$$\|(S^r \otimes S^l)^\top e_t\|_2 = \|\text{vec}(S^{l\top} E_t S^r)\|_2 = \|S^{l\top} E_t S^r\|_F \leq \|E_t\|_F \quad (26)$$

Here E_t is the matrix form of e_t , and as declared before, $e_t := (a_t - a_{t-1}) + (D_{t-1} - D_t) w_t$, thus:

$$E_t := \frac{1}{N} \sum_i (A_{i,t} - A_{i,t-1}) + \frac{1}{N} \sum_i (B_{i,t-1} W_t C_{i,t-1} - B_{i,t} W_t C_{i,t}) \quad (27)$$

Next, we need to find an upper bound for the norm of each term in (27) to establish an upper bound for $\|E_t\|_F$. Based on the assumptions of the theorem, A_i , B_i , and C_i exhibit L-Lipschitz continuity with constants L_A , L_B , and L_C , respectively. Additionally, $\|W_t\|_F$ is bounded by a scalar M . We have:

$$\|A_t - A_{t-1}\|_F \leq L_A \|W_t - W_{t-1}\|_F = \mu L_A \|\tilde{G}_{t-1}\|_F \leq \mu L_A \|P_{t-1}\|_F \quad (28)$$

In the first equality, we apply (13), while the last equality holds due to (20) and the orthonormality of the projection matrices. The subsequent two inequalities can be derived similarly using these equations.

$$\begin{aligned}
\|(B_t - B_{t-1}) W_t C_{t-1}\|_F &\leq L_B \|W_t - W_{t-1}\|_F \|W_t\|_F \|C_{t-1}\|_F \\
&= \mu L_B L_C M^2 \|P_{t-1}\|_F
\end{aligned} \quad (29)$$

$$\begin{aligned}
\|B_t W_t (C_{t-1} - C_t)\|_F &\leq L_C \|B_t\|_F \|W_t\|_F \|W_{t-1} - W_t\|_F \\
&= \mu L_B L_C M^2 \|P_{t-1}\|_F
\end{aligned} \quad (30)$$

We can now derive the bound for $\|E_t\|_F$ as follows:

$$\begin{aligned}
\|E_t\|_F &\leq \mu L_A \|\tilde{G}_{t-1}\|_F \leq \mu L_A \|P_{t-1}\|_F + \mu L_B L_C M^2 \|P_{t-1}\|_F + \mu L_B L_C M^2 \|P_{t-1}\|_F \\
&= \mu (L_A + 2L_B L_C M^2) \|P_{t-1}\|_F
\end{aligned} \quad (31)$$

To calculate the norm bound for the first term in (25), we first need to establish the bounds for \widehat{D}_t . This involves estimating the minimum eigenvalue of \widehat{D}_t .

If we define $\gamma_{min,i,t} = \lambda_{min}(S^{l\top} B_{i,t} S^l) \lambda_{min}(S^{r\top} C_{i,t} S^r)$, then it follows that $\lambda_{min}((S^{l\top} B_{i,t} S^l) \otimes (S^{r\top} C_{i,t} S^r)) = \gamma_{min,i,t}$. Consequently, \widehat{D}_t will satisfy the following inequality for every unit vector \vec{v} :

$$\vec{v}^\top \widehat{D}_t \vec{v} = \frac{1}{N} \sum_i \vec{v}^\top \left[(S^{l\top} B_{i,t} S^l) \otimes (S^{r\top} C_{i,t} S^r) \right] \vec{v} \geq \frac{1}{N} \sum_i \gamma_{min,i,t} \quad (32)$$

this actually provides a lower bound for eigenvalues of \widehat{D}_t , thus:

$$\lambda_{\max}(I - \mu \widehat{D}_{t-1}) \leq 1 - \frac{\mu}{N} \sum_i \gamma_{min,i,t-1} \quad (33)$$

considering the definition of κ_t in the theorem, we can now easily show that:

$$\|P_t\|_F \leq [1 - \mu(\kappa_{t-1} - L_A - 2L_B L_C M^2)] \|P_{t-1}\|_F.$$

and completing the proof.

While SubTrack++ utilizes right/left projections to reduce memory consumption, the proof is presented using both projection matrices to ensure generality. Here, we demonstrate how the proof proceeds under the assumption $m \leq n$ (without loss of generality), which allows the use of the left projection matrix.

Using the left projection matrix, the current formulation of P_t , defined as $P_t = S_t^{l\top} G_t S_t^r$, simplifies to $P_t = S_t^{l\top} G_t$. Similarly, $\widehat{G}_t = S_t^l S_t^{l\top} G_t S_t^r S_t^{r\top}$ reduces to $\widehat{G}_t = S_t^l S_t^{l\top} G_t$. From this point, the proof continues by substituting S_t^r with the identity matrix, allowing the derivation of the vectorized forms of g_t, \widehat{g}_t, p_t , and related terms.

The remainder of the proof remains largely unaffected. It can be readily verified that the recursive formulation of g_t is unchanged. Although the definition of P_t is modified, it continues to satisfy the bounds required for convergence, ensuring that P_t converges to 0 when the left projection matrix is used.

B Grassmann Exponential

Theorem 3.6 (Grassmann Exponential). *Let $P = UU^\top \in Gr(n, p)$ be a point on the Grassmannian, where $U \in St(n, p)$ is the orthonormal basis of the corresponding subspace. Consider a tangent vector $\Delta \in T_P Gr(n, p)$, and let Δ_V^{hor} denote the horizontal lift of Δ to the horizontal space at U in the Stiefel manifold $St(n, p)$. Suppose the thin SVD of Δ_V^{hor} is given by $\Delta_V^{hor} = \widehat{Q} \Sigma V^\top$, where $\widehat{Q} \in St(n, r)$, $\Sigma = \text{diag}(\sigma_1, \dots, \sigma_r)$ contains the nonzero singular values of Δ_V^{hor} with $r = \min(p, n - p)$, and $V \in St(p, r)$. The Grassmann exponential map, representing the geodesic emanating from P in the direction Δ , is given by:*

$$\text{Exp}_P^{Gr}(t\Delta) = [UV \cos(t\Sigma) V^\top + \widehat{Q} \sin(t\Sigma) V^\top + UV_\perp V_\perp^\top],$$

where $V_\perp \in \mathbb{R}^{p \times (p-r)}$ is any orthogonal complement of V .

proof. Using Grassmannina mathematics, we know that every $\Delta \in T_P Gr(n, p)$ is of the form

$$\Delta = Q \begin{pmatrix} 0 & B^\top \\ B & 0 \end{pmatrix} Q^\top = \left[Q \begin{pmatrix} 0 & -B^\top \\ B & 0 \end{pmatrix} Q^\top, P \right] \quad (34)$$

Then the lift of $\Delta \in T_P Gr(n, p)$ to $Q = (U \ U_\perp)$ can also be calculated explicitly as follows:

$$\Delta_Q^{hor} = [\Delta, P]Q = Q \begin{pmatrix} 0 & -B^\top \\ B & 0 \end{pmatrix} \quad (35)$$

To resume our proof, we need to define the orthogonal group and specifying its tangent space.

Definition B.1 (Orthogonal Group). The orthogonal group $O(n)$ is defined as the set of all $n \times n$ matrices Q over \mathbb{R} such that $Q^\top Q = QQ^\top = I_n$, where Q^\top is the transpose of Q and I_n is the $n \times n$ identity matrix:

$$O(n) = \{Q \in \mathbb{R}^{n \times n} \mid Q^\top Q = I_n = QQ^\top\}.$$

Then the tangent space of the orthogonal group $O(n)$ at a point Q , denoted $T_Q O(n)$, is defined as the set of matrices of the form $Q\Omega$, where $\Omega \in \mathbb{R}^{n \times n}$ is a skew-symmetric matrix, i.e., $\Omega^\top = -\Omega$:

$$T_Q O(n) = \{Q\Omega \mid \Omega \in \mathbb{R}^{n \times n}, \Omega^\top = -\Omega\}.$$

The geodesic from $Q \in O(n)$ in direction $Q\Omega \in T_Q O(n)$ is calculated via

$$\text{Exp}_Q^O(tQ\Omega) = Q \exp_m(t\Omega), \quad (36)$$

If $P \in Gr(n, p)$ and $\Delta \in T_P Gr(n, p)$ with $\Delta_Q^{\text{hor}} = Q \begin{pmatrix} 0 & -B^\top \\ B & 0 \end{pmatrix}$, the geodesic in the Grassmannian is therefore

$$\text{Exp}_P^{Gr}(t\Delta) = \pi^{OG} \left(Q \exp_m \left(t \begin{pmatrix} 0 & -B^\top \\ B & 0 \end{pmatrix} \right) \right). \quad (37)$$

where π^{OG} is the projection from $O(n)$ to $Gr(n, p)$. If the thin SVD of B is given by

$$B = U_\perp^\top \Delta_U^{\text{hor}} = U_\perp^\top \hat{Q} \Sigma V^\top$$

with $W := U_\perp^\top \hat{Q} \in St(n-p, r)$, $\Sigma \in \mathbb{R}^{r \times r}$, $V \in St(p, r)$. Let W_\perp, V_\perp be suitable orthogonal completions. Then,

$$\exp_m \begin{pmatrix} 0 & -B^\top \\ B & 0 \end{pmatrix} = \begin{pmatrix} V & V_\perp & 0 & 0 \\ 0 & 0 & W & W_\perp \end{pmatrix} \begin{pmatrix} \cos(\Sigma) & 0 & -\sin(\Sigma) & 0 \\ 0 & I_{p-r} & 0 & 0 \\ \sin(\Sigma) & 0 & \cos(\Sigma) & 0 \\ 0 & 0 & 0 & I_{n-p-r} \end{pmatrix} \begin{pmatrix} V^\top & 0 \\ V_\perp^\top & 0 \\ 0 & W^\top \\ 0 & W_\perp^\top \end{pmatrix},$$

which leads to the desired result when inserted into (37). For more mathematical details, you can refer to Edelman et al. [1998], Bendokat et al. [2024], or other useful resources on Grassmann geometry.

C Projection-Aware Optimizer

When projecting into a lower-dimensional space and tracking coordinate changes, we typically use orthonormal projection matrices to represent the subspaces and their multiplications to effect a change of basis. While this works well for purely linear operations, Adam's updates also incorporate non-linear elements.

Suppose the subspace changes at step t , transitioning from the subspace spanned by the orthonormal matrix S_{t-1} to that spanned by S_t . Since both matrices are orthonormal—preserved by the Grassmannian update rule in (5)—the matrix $S_t^\top S_{t-1}$ represents the change of basis between the two subspaces. In other words, if $\mathbb{E}_{t-1} = (e_{t-1}^1, \dots, e_{t-1}^r)$ and $\mathbb{E}_t = (e_t^1, \dots, e_t^r)$ are orthonormal bases for the subspaces at steps $t-1$ and t , respectively, then the i th column of matrix X transforms under the change of basis as $X_t^i = \sum_{j=1}^r \langle e_t^i, e_{t-1}^j \rangle X_{t-1}^j$, where X_{t-1}^j is the j th column of X based on the basis of the time step $t-1$.

$\mathbf{E}_{t,\beta}[\cdot]$ denotes the exponential time-weighted expectation at time t with decay rate β . Following the reinterpretation by Robert et al. [2025], Adam's first and second moment estimates can be expressed as $\tilde{M}_t = \mathbf{E}_{t,\beta_1}[\tilde{G}_t]$ and $\tilde{V}_t = \mathbf{E}_{t,\beta_2}[(\tilde{G}_t)^2]$, where \tilde{G}_t denotes the low-rank representation of the gradient at time step t . As shown in (38), the first moment estimate can be transformed under a change of basis using the change-of-basis matrix, $S_t^\top S_{t-1}$. Notably, $\langle \tilde{G}_t, e_t^i \rangle$ gives the i th column of \tilde{G}_t when the subspace has the basis \mathbb{E}_t . We use the superscripts to indicate a column of a matrix.

$$\mathbf{E}_{t,\beta_1}[\langle \tilde{G}_t, e_t^i \rangle] = \sum_{j=1}^r \langle e_t^i, e_{t-1}^j \rangle \mathbf{E}_{t,\beta_1}[\langle \tilde{G}_t, e_{t-1}^j \rangle] = \sum_{j=1}^r \langle e_t^i, e_{t-1}^j \rangle \tilde{M}_t^j = \left(S_t^\top S_{t-1} \tilde{M}_t \right)^i \quad (38)$$

Following the same approach, we can change the basis for the second moment estimate as described in (39).

$$\begin{aligned}
\mathbf{E}_{t,\beta_2} \left[\left(\langle \tilde{G}_t, e_t^i \rangle \right)^2 \right] &= \sum_{j=1}^r \langle e_t^i, e_{t-1}^j \rangle^2 \mathbf{E}_{t,\beta_2} \left[\left(\langle \tilde{G}_t, e_{t-1}^j \rangle \right)^2 \right] \\
&\quad + \sum_{k \neq l}^r \langle e_t^i, e_{t-1}^k \rangle \langle e_t^i, e_{t-1}^l \rangle \mathbf{E}_{t,\beta_2} \left[\langle \tilde{G}_t, e_{t-1}^k \rangle \langle \tilde{G}_t, e_{t-1}^l \rangle \right] \\
&= \sum_{j=1}^r \langle e_t^i, e_{t-1}^j \rangle^2 \tilde{\mathcal{V}}_t^j \\
&\quad + \sum_{k \neq l}^r \langle e_t^i, e_{t-1}^k \rangle \langle e_t^i, e_{t-1}^l \rangle \tilde{M}_t^k \tilde{M}_t^l.
\end{aligned} \tag{39}$$

In transitioning from the first equality to the second, we assume independence among the gradient coordinates. This enables us to approximate the covariance using a product of first-order moment estimates. This assumption is often reasonable in practice because we compute the SVD of the gradient and maintain an orthonormal subspace projection matrix, updating it along the Grassmannian geodesic to track the optimal subspace. Since SVD tends to diagonalize the covariance, the off-diagonal entries are typically negligible. Additionally, we clip any negative values to zero to ensure valid (non-negative) variance estimates. Moreover, to rewrite the second term in the final equality of (39), we employ the following equation:

$$\begin{aligned}
&\sum_k \sum_l \langle e_t^i, e_{t-1}^k \rangle \langle e_t^i, e_{t-1}^l \rangle \tilde{M}_t^k \tilde{M}_t^l \\
&= \sum_k \langle e_t^i, e_{t-1}^k \rangle^2 \left(\tilde{M}_t^k \right)^2 + \sum_{k \neq l} \langle e_t^i, e_{t-1}^k \rangle \langle e_t^i, e_{t-1}^l \rangle \tilde{M}_t^k \tilde{M}_t^l
\end{aligned} \tag{40}$$

Given these, we can rewrite (39) as follows:

$$\begin{aligned}
\mathbf{E}_{t,\beta_2} \left[\langle \tilde{G}_t, e_t^i \rangle^2 \right] &= \sum_j \langle e_t^i, e_{t-1}^j \rangle^2 \tilde{\mathcal{V}}_t^j + \\
&\quad \left[\sum_k \sum_l \langle e_t^i, e_{t-1}^k \rangle \langle e_t^i, e_{t-1}^l \rangle \tilde{M}_t^k \tilde{M}_t^l - \sum_k \langle e_t^i, e_{t-1}^k \rangle^2 \left(\tilde{M}_t^k \right)^2 \right] \\
&= \sum_j \langle e_t^i, e_{t-1}^j \rangle^2 \left[\tilde{\mathcal{V}}_t^j - \left(\tilde{M}_t^j \right)^2 \right] + \left(\langle e_t^i, e_{t-1}^j \rangle \tilde{M}_t^j \right)^2 \\
&= \left(\left(S_t^\top S_{t-1} \right)^2 \left[\tilde{\mathcal{V}}_t - \tilde{M}_t^2 \right] \right)^i + \left(\left(S_t^\top S_{t-1} \tilde{M}_t \right)^2 \right)^i
\end{aligned} \tag{41}$$

By applying (38) and (41), we can directly derive the update rules for the projection-aware optimizer, as expressed in (8) and (9).

D Time Complexity Analysis

Table 3 presents the time complexity breakdown for the subspace update step in the SubTrack++ algorithm assuming a $m \times n$ gradient matrix and rank r projection matrix, where $r \ll m \leq n$. As outlined in Algorithm 1, the subspace update step begins by solving the least squares problem (2) to estimate the optimal update for S_t , the $m \times r$ orthonormal matrix. This operation has a time complexity of $O(mr^2)$. Computing the residual and the partial derivative with respect to S_t requires $O(mrn)$ and $O(mnr)$ time respectively. This is because the solution to the least squares problem, A , has shape $r \times n$ which is multiplied by S_t in the residual $R = G_t - S_t A$, resulting in time complexity $O(mrn)$. The following operation for the partial derivative is $-2RA^T$, where the matrix multiplication has $O(mnr)$ complexity. The tangent vector computation (4) which involves an identity transformation and matrix multiplication has time complexity of $O(m^2r)$.

The rank-1 approximation step uses largest singular value from the SVD of the $m \times r$ tangent vector, and has time complexity of $O(mr^2)$. Finally, the update rule as shown in (13) which has a time complexity of $O(mr^2)$. The overall complexity of the algorithm is dominated by the matrix multiplication calculations of time complexity $O(mnr)$. However, unlike GaLore, since we avoid computing SVD operation on the $m \times n$ gradient matrix, which has complexity of $O(nm^2)$, the overall update step in SubTrack++ is still more efficient with respect to time complexity.

Table 3: Time Complexity for SubTrack++ Subspace Update

Computation Step	Time
Cost function	$O(mr^2)$
Residual	$O(mrn)$
Partial derivative	$O(mnr)$
Tangent vector ΔF	$O(m^2r)$
Rank-1 approximation of ΔF	$O(mr^2)$
Update rule	$O(mr^2)$
Overall	$O(mnr)$

E Fine-Tuning Experiments

As described, we examined SubTrack++ on fine-tuning RoBERTa-base and RoBERTa-large models to evaluate them on GLUE and SuperGLUE benchmarks. The results for GLUE task is summarized in Table 4, and SuperGLUE in 5.

Table 4: Evaluating the performance of SubTrack++ and other baselines when fine-tuning RoBERTa-Base on GLUE tasks for $r = 8$. The performance is measured via Accuracy for SST-2 and RTE tasks, F1 for MRPC, Pearson Correlation for STS-B, and Matthews Correlation for COLA. The best results are marked in **bold**, with the second-best performance underlined.

	COLA	STS-B	MRPC	RTE	SST-2
Full-Rank	62.57	91.03	91.32	77.98	94.27
BAdam [Luo et al., 2024]	54.44	89.01	91.35	68.59	94.15
GaLore [Zhao et al., 2024]	<u>58.54</u>	<u>90.61</u>	91.30	<u>74.37</u>	94.50
LDAdam [Robert et al., 2025]	58.81	90.90	92.22	76.53	<u>94.27</u>
SubTrack++ (Ours)	58.29	90.90	<u>91.84</u>	76.53	90.83

Table 5: Evaluating the performance of SubTrack++ and other baselines when fine-tuning RoBERTa-Large on SuperGLUE tasks with $r = 8$. The performance is measured via Accuracy for COPA, WIC, WSC, BoolQ, and AX_g tasks, and F1 for CB. The best results are marked in **bold**, with the second-best performance underlined.

	BoolQ	CB	COPA	WIC	WSC	AX _g
Full-Rank	85.96	90.33	76.00	71.79	63.46	96.30
GaLore [Zhao et al., 2024]	<u>85.44</u>	<u>88.85</u>	<u>80.00</u>	71.47	<u>63.46</u>	100.00
BAdam [Luo et al., 2024]	82.51	53.28	59.00	70.38	60.58	51.85
LDAdam Robert et al. [2025]	85.75	56.16	<u>80.00</u>	<u>71.00</u>	64.42	<u>70.37</u>
SubTrack++ (Ours)	84.68	89.66	88.00	70.06	<u>63.46</u>	100.00

The hyperparameters for fine-tuning RoBERTa-base are detailed in Table 6, matching those reported in the GaLore [Zhao et al., 2024] for rank-8 subspaces, with a subspace update interval set at 500 iterations. We also fine-tuned RoBERTa-Large on SuperGLUE tasks using the hyperparameters from Luo et al. [2024], as detailed in Table 7, with the exception that we fine-tuned each task for 30 epochs.

Table 6: Hyperparameters of fine-tuning RoBERTa-Base on GLUE tasks.

		SST-2	MRPC	CoLA	RTE	STS-B
Shared Parameters	Batch Size	16	16	32	16	16
	# Epochs			30		
	Max Seq. Len.			512		
Low-Rank Optimizer Methods Parameters	Learning Rate	2E-05	2E-05	1E-05	2E-05	3E-05
	SubTrack Step-Size	0.01	3.0	5.0	15.0	10.0
	Subspace Update Interval			500		
	Rank Config			8		
	α			2		
BAdam Parameters	Learning Rate	2E-05	2E-05	1E-05	2E-05	3E-05
	Block Switch Interval			100		
	Switch Mode			Random		

Table 7: Hyperparameters of fine-tuning RoBERTa-Large on SuperGLUE tasks.

		BoolQ	CB	COPA	WIC	WSC	AX _g
Shared Parameters	Batch Size				16		
	# Epochs				30		
	Learning Rate				1e-5		
	Max Seq. Len.				512		
Low-Rank Optimizer Methods Parameters	SubTrack++ Step-Size	0.1	1.0	50.0	100.0	1.0	1.0
	Subspace Update Interval	500	100	100	500	250	100
	Rank Config.				8		
	α				4		
	BAdam Parameters	Block Switch Interval	100	50	50	100	50
Switch Mode					Random		

F Memory and Time Comparison

Table 8 presents the the peak memory consumption measured to compare SubTrack++ and other baselines. It shows that SubTrack++ requires on-par or better memory compared to GaLore [Zhao et al., 2024] and Fira [Chen et al., 2025] while getting state-of-the-art results. As detailed in Table 2, all baselines except BAdam [Luo et al., 2024] use the same number of optimizer parameters; therefore, any differences in their peak memory consumption stem from variations in their runtime parameters.

Additionally, Table 9 presents the wall-time consumed by each baseline across all model architectures during pre-training. Each run is configured to include exactly 10 subspace updates for SubTrack++ and other baselines employing periodic subspace updates. Specifically, models ranging from 60M to 3B use a subspace update interval of 200, resulting in 2,000 total iterations, while the 7B models use an interval of 500, yielding 5,000 iterations. Experiments for the 60M to 3B models are conducted on an NVIDIA A100 GPU, while the 7B model experiments are run on an NVIDIA RTX A6000.

G Pre-Training Llama-Based Architectures

We pre-trained all six Llama-based architectures for 10,000 iterations using hyperparameters reported in Table 10. Hyperparameters are selected based on reported values in GaLore paper [Zhao et al., 2024].

H Subspace Tracking vs. SVD

Replacing SVD with Grassmannian-based subspace tracking, as opposed to the approach used in GaLore [Zhao et al., 2024] and Fira [Chen et al., 2025], offers two key advantages: (1) Robustness:

Table 8: Peak memory consumption comparison when pre-training Llama-based architectures with different sizes on C4 dataset. The 7B models are trained using the 8-bit Adam optimizer, except for the runs marked with *. SubTrack++ demonstrates better or on-par memory compared to other low-rank methods that allows full-parameter training.

	60M r=128	130M r=256	350M r=256	1B r=512	3B r=512	7B r=1024
Full-Rank	16.86	25.32	28.67	18.83	34.92	50.50
BAdam [Luo et al., 2024]	13.34	20.01	16.45	9.18	14.75	22.35
GaLore [Zhao et al., 2024]	16.89	25.52	27.85	14.74	26.03	36.00
Online Subspace Descent Liang et al. [2024]	16.61	25.86	28.76	18.45	32.57	33.10
LDAdam [Robert et al., 2025]	17.18	25.94	28.03	18.45	32.57	OOM*
Fira [Chen et al., 2025]	16.39	24.99	27.33	14.68	25.62	47.84*
SubTrack++ (Ours)	16.40	25.06	27.42	15.22	25.54	49.82*

Table 9: Wall-time comparison for pre-training LLaMA-based architectures of varying sizes on the C4 dataset. The number of iterations is set to ensure 10 subspace updates for methods using periodic subspace updates: 2k for models ranging from 60M to 3B, and 5k for the 7B model. SubTrack++ achieves the lowest wall-time among all baselines that support full-parameter training on large models. The 7B models are trained using the 8-bit Adam optimizer, except for the runs marked with *. Since this can impact wall-time comparisons, it is more appropriate to compare runs within the same cluster.

	60M r=128	130M r=256	350M r=256	1B r=512	3B r=512	7B r=1024
Full-Rank	524.0	1035.1	1396.4	974.9	1055.9	12726.2
BAdam [Luo et al., 2024]	511.3	779.2	961.6	798.6	1004.1	7283.7
GaLore [Zhao et al., 2024]	547.8	1094.2	1589.0	1729.5	2715.5	21590.4
Online Subspace Descent [Liang et al., 2024]	662.8	1228.2	1818.6	1438.7	1676.9	21590.4
LDAdam [Robert et al., 2025]	639.9	1342.2	2083.4	2780.9	4625.4	OOM*
Fira [Chen et al., 2025]	635.3	1180.8	1729.7	1938.5	2898.4	22554.3*
SubTrack++ (Ours)	627.6	1140.6	1593.2	1304.3	1517.6	16491.7*

As shown in Figure 5, Grassmannian tracking better handles noise and abrupt shifts, preserving subspace quality under dynamic conditions. (2) Efficiency: It significantly reduces computational overhead (see Table 2 and Appendix D). Figure 6 illustrates the wall-time of the experiments in the ablation in Figure 3, highlighting substantial speedups.

As a result, SubTrack++ achieves SOTA-level performance with GaLore-like memory use, while being one of the fastest methods; clearly demonstrated in Figure 4 and 6.

Table 10: Hyperparameters of pre-training Llama-based architectures.

		60M	130M	350M	1B	3B	7B
Architectural Parameters	Hidden	512	768	1024	2048	2560	4096
	Intermediate	1376	2048	2736	5461	6848	11008
	Heads	8	12	16	24	32	32
	Layers	8	12	24	32	32	32
Shared Parameters	Learning Rate	1e-3	1e-3	1e-3	1e-4	1e-4	1e-4
	Batch Size	128	128	64	8	8	4
	Gradient Accumulation	2	2	2	2	2	4
	Iterations				10K		
	Gradient Clipping				1.0		
	Warmup Steps				1000		
	scale dtype				0.25 bfloat16		
Low-Rank Optimizer Methods Parameters	Rank	128	256	256	512	512	1024
	Subspace Update Interval	200	200	200	200	200	500
	SubTrack++ Step-Size				10		
BAdam Parameters	Block Switch Interval				100		
	Switch Mode				Random		

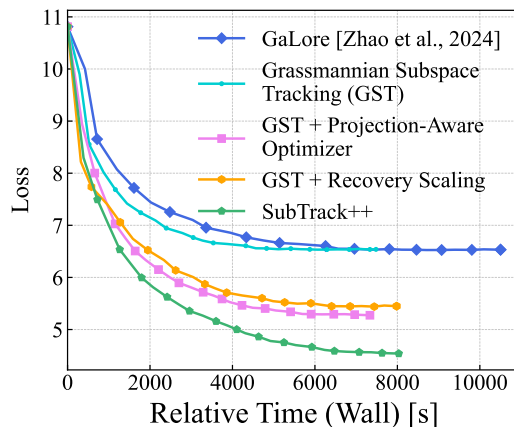


Figure 6: Ablation study comparing pure Grassmannian subspace tracking with incremental additions of the projection-aware optimizer and recovery scaling, leading to SubTrack++ . Grassmannian tracking exceeds GaLore’s convergence, and significantly reduces wall-time, as also shown in Figure 4.